

Sharp Fringes Using Cascaded Multiple Beam Interferometers- Application on Kidney Images

A.M. Hamed

Physics Department, Faculty of Science,
Ain Shams University, 11566 Cairo, Egypt.
e- mail : amhamed73@hotmail.com

ABSTRACT

In this paper, a new set up of multiple beam interference is considered using Cascaded Fabry Perot Interferometer (CFPI). An application of this CFPI on kidney images is given. The sharp fringes are deformed by the kidney phase giving modulated fringes. The sharp fringe shift of the kidney images obtained in case of the multipass model of CFPI is investigated. In addition, the image contrast is compared with the contrast in case of ordinary FPI. Finally, the modulated two beam interference of kidney images is given.

Key words: Cascaded Fabry Perot Interferometer. Modulated interference fringes. Image contrast.

1. INTRODUCTION

The idea of multipassed FPI was early suggested in [1]. Later, a double Fabry- Perot interferometer was designed in order to improve the fringe contrast giving contrast nearly 30 times the contrast of a single FPI [2]. Image processing of biomedical images is useful in the investigation of images, in particular for ultra- sonic medical images provided with multiplicative speckle noise filtering is important to get rid of the noise using for example Wiener or Median filtering. The mean filter is not useful for multiplicative noise. The development of a semi-automated program that used image processing techniques and geometry principles to define the boundary, and segmentation of the kidney area, and to enhance kidney stone detection [3- 5].The Discrete Wavelet Transform (DWT) is attractive for de-noising since it has the advantage of varying the scale at which the component frequencies are analyzed [6- 8] as compared with the Fourier transform techniques. Hence, speckle noising which is multiplicative is decreased giving S/N ratio in the DWT better than the corresponding S/N ratio in case of Wiener and Median filters. Recently, as outlined in [9], the wavelet de-noising involves the following stages: calculate the DWT, remove noise by changing the wavelet coefficients, and apply the inverse (IDWT) to construct the de-speckled image. Another method of improving the ultra- sonic low contrast kidney images based on reduction of

speckle noise using Gabor filter, then the de-speckled image is enhanced using histogram equalization [10]. Image processing of some biomedical images are presented using two beam and ordinary multiple beam techniques[11- 13]leading to extract phase information from the images. In this study, sharp interferometric images produced from the sequence of the interferometers using CFPI as compared with the ordinary FPI is shown. The phase information of kidney images obtained from the modulated interference images are obtained. In a recent publication by the author [14], we consider multiple pass of two beam interference, while in this study we consider CFPI arranged in series.

2. A CASCADED FABRY-PEROT INTERFEROMETER (CFPI)

A higher order multiple beam interference composed of four cascaded interferometers schematically represented as in the figure (1). A He- Ne laser beam is spatially filtered and rendered parallel using an objective lens L followed by a pinhole P placed in the short focus of the objective lens, and converging lens L_1 placed at the focal plane f from the pinhole. The collimated laser beam passes through the four F.P.I. arranged in series followed by the Fourier transform lens L_2 of focal length f_2 , The Fourier and imaging planes are located as shown in the figure (1).

The intensity distribution in case of ordinary FPI is given by this formula [11]:

$$I(\delta; R) = \frac{T^4}{1 + R^4 - 2R^2 \cos \delta} \quad (1)$$

Where T is the transmission coefficient while R is the reflection coefficient of the interferometer. δ , is the phase difference between any two adjacent emerging rays. While in case of cascaded interferometers, the intensity distribution is the ordinary distribution to the power of N, where N is the number of cascaded interferometers. Then, the intensity distribution is represented as follows:

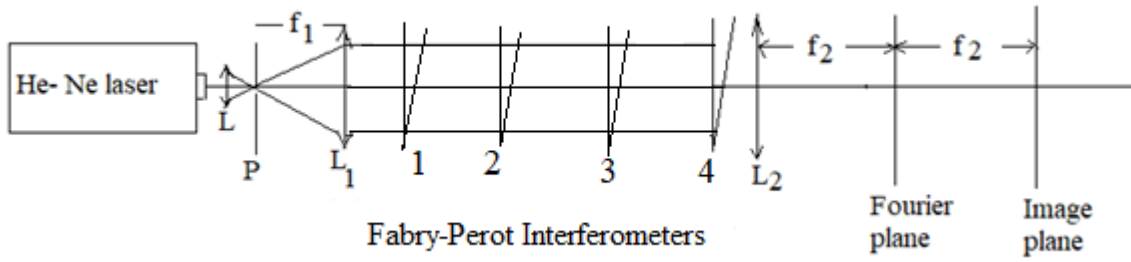


Figure (1): Multiple beam interferometer composed of four cascaded interferometers. L objective lens, P pinhole, and L1 converging lens where the elements L, P, and L1 render the laser beam spatially filtered and collimated. L2 is the Fourier transform lens of focal length f2, The Fourier and imaging planes are shown in the figure.

$$I(\delta; R, N) = \left[\frac{T^4}{1 + R^4 - 2R^2 \cos(\delta)} \right]^N \quad (2)$$

The maximum intensity is computed as:

$$I(\delta = 2\pi; R, N) = I_{max}(R, N) = \left[\frac{T^4}{(1 - R^2)^2} \right]^N \quad (3)$$

Making use of equations (2, 3), the normalized intensity due to the cascaded multiple beam interference can be written as follows:

$$I_{normalized}(\delta; R, N) = \frac{I}{I_{max}} = \frac{1}{\left[1 + F \sin^2\left(\frac{\delta}{2}\right) \right]^N} \quad (4)$$

Where $F = \frac{4R^2}{(1 - R^2)^2}$ is the coefficient of finesse.

(5)

F is a measure of fringe sharpness and contrast.

For greater values of reflectivity, $R > 80\%$, F is much larger than one, hence, approximate expression for the intensity is obtained as:

$$I_{normalized}(\delta; R, N) \sim 1 / \left[F \sin^2\left(\frac{\delta}{2}\right) \right]^N \quad (6)$$

3. RESULTS AND DISCUSSION

The coefficient of finesse F as a function of reflectivity R for different cascaded interferometers is computed from equation (6) and represented as shown in the figure (2). N=1 stands for the ordinary FPI while N= 2, 3, and 4 stands for the number of cascaded interferometers. In the left, a normal kidney image while in the right, a polycystic kidney is shown as in the figure (3). This image is extracted from the following site: www.kidneyfailure.com. Kidney failure is investigated using two- beam interference. In the left side, nearly regular shift is shown for the normal kidney while irregular random shift is obtained in the right side corresponds to the kidney failure as shown in the figure (4- a), where M = 15. The details of the irregular shift for the kidney failure are shown using higher number of interference fringes M = 60, as shown in the figure (4- b). two- beam interference. In the left side, nearly regular shift is shown for the normal kidney while irregular random shift is obtained in the right side corresponds to the kidney failure as shown in the figure (4- a), where M = 15. The details of the irregular shift for the kidney failure are shown using higher number of interference fringes M = 60, as shown in the figure (4- b). A segment from the normal kidney modulated by two beam interference is shown in figure (5- a), while a segment of failure kidney modulated by two beam interference is shown in the figure (5- b). Another plot of both failure kidney as in the figure (6) showed random interference within the kidney as shown in the figure (7). A plot of normal and cancerous kidney shown as in the figure (8 a, b). A normal kidney modulated by two beam interference fringes is shown in the figure (9- a), while the cancerous kidney modulated by interference showed contour encircled the cancerous part as shown in the figure (9- b). The modulated cancerous part from the kidney is shown in the figure (9- c).

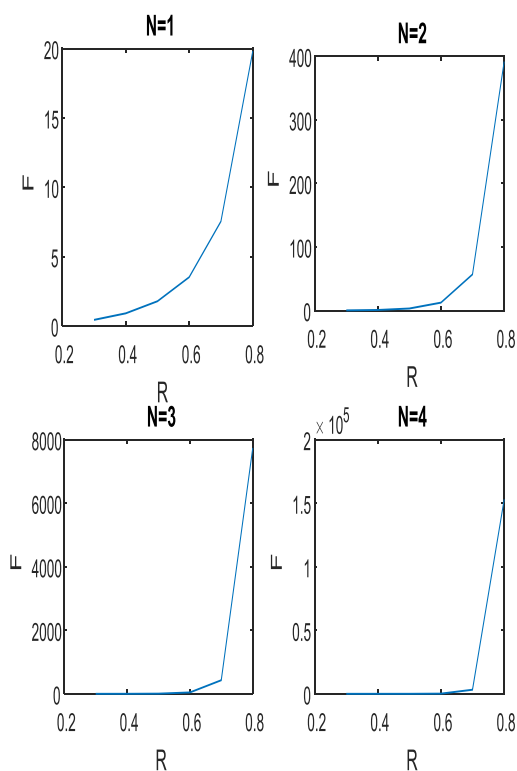


Figure (2): Coefficient of finesse F as a function of reflectivity R for different cascaded interferometers. $N=1$ stands for the ordinary FPI while $N= 2, 3,$ and 4 stands for the number of cascaded interferometers.

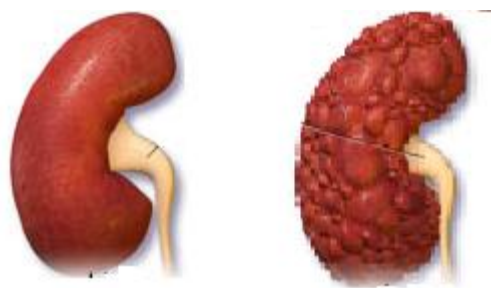


Figure (3): in the left, a normal kidney image while in the right, a polycystic kidney is shown. This image is extracted from the following site: www.kidneyfailure.com

The ordinary F P I where the number of interferometers $N=1$, is shown as in the figure (10- a). The cancerous kidney shown in the figure (8- b) is modulated by 30 fringes. The cascaded higher orders of F P I modulated the cancerous kidney are shown in the figures (10 b, c, d). In all the figures irregular segment shown in the upper part of the kidney represents the cancerous part. The cascaded arrangement of F P I modulated by the image is computed

from equation (6), where the image matrix is introduced in the modulation interference phase term.

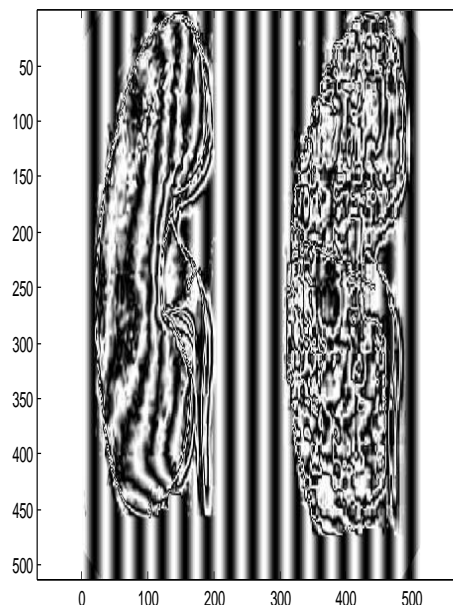


Figure (4- a): Kidney failure is investigated using two-beam interference. In the left side, nearly regular shift is shown for the normal kidney while irregular random shift is obtained in the right side corresponds to the kidney failure. The number of fringes (M)= 15.

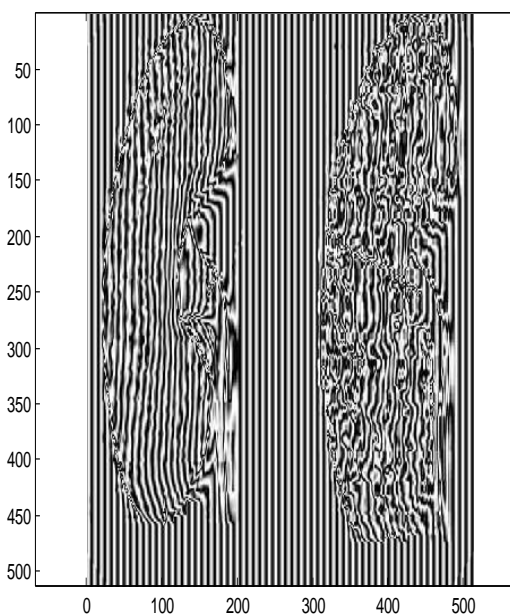


Figure (4- b): Kidney failure is investigated using two-beam interference. In the left side, nearly regular shift is shown for the normal kidney while irregular random shift is shown in the right side corresponds to the kidney failure. Number of fringes(M) = 60.

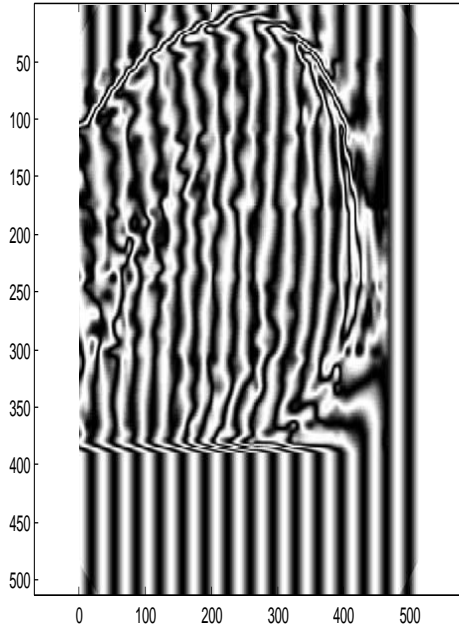


Figure (6): It is shown in the figure that both kidneys have a failure.

Figure (5- a): Segment of normal kidney modulated by two beam interference

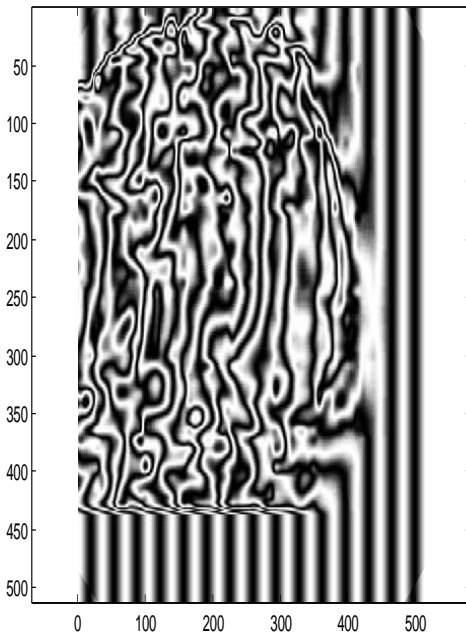


Figure (5- b): Segment of failure kidney modulated by two beam interference.

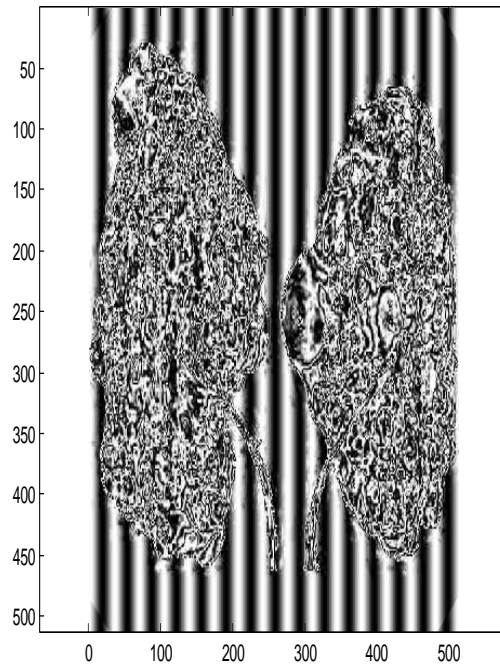
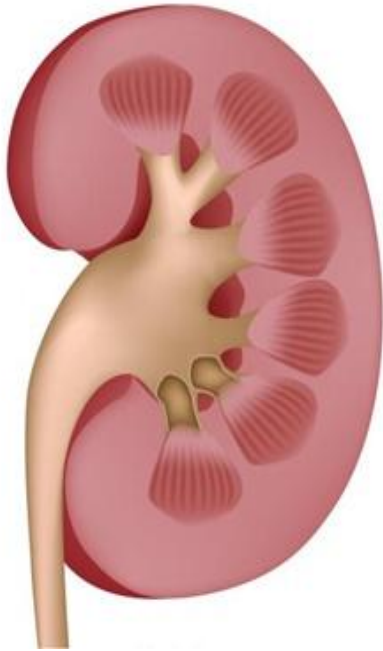


Figure (7): It is shown in the modulated interference that both kidneys have a failure outlined by the randomness in the interference pattern.



Figure(8-a): Normal kidney image of dimensions 552× 438 pixels

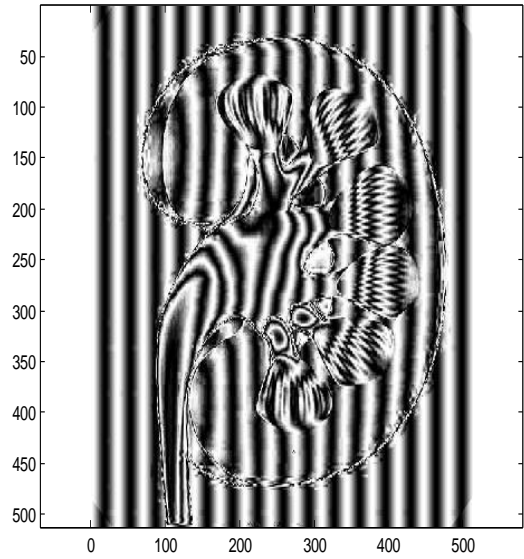
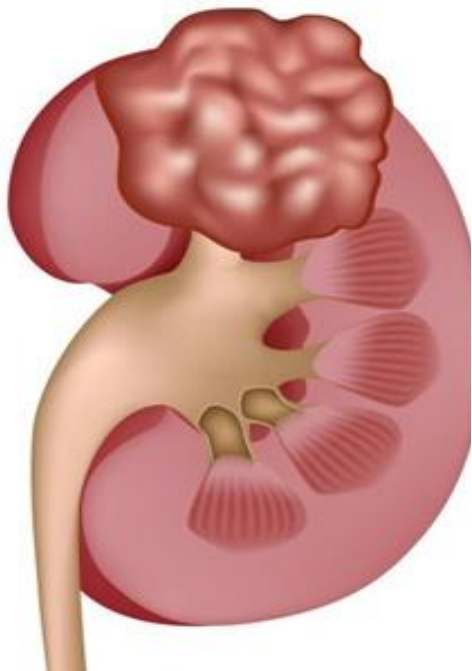


Figure (9-a): Normal kidney modulated by two beam interference fringes



Figure(8-b): Cancerous kidney image of dimensions 552× 438 pixels

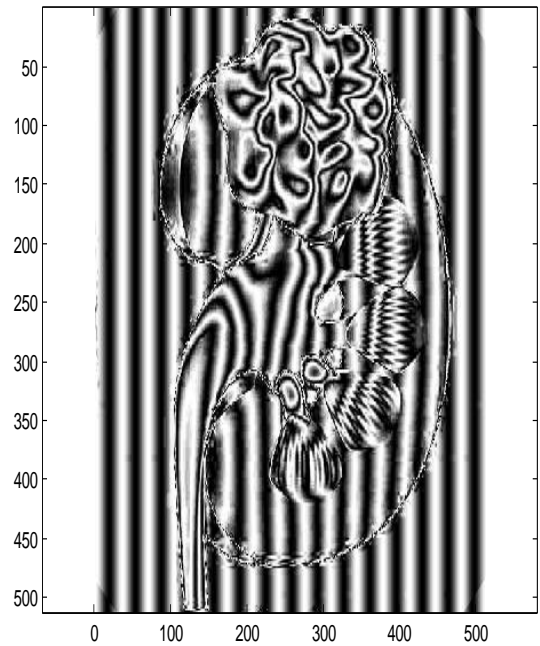


Figure (9- b): Contour fringes shown in the upper part of the cancerous kidney.

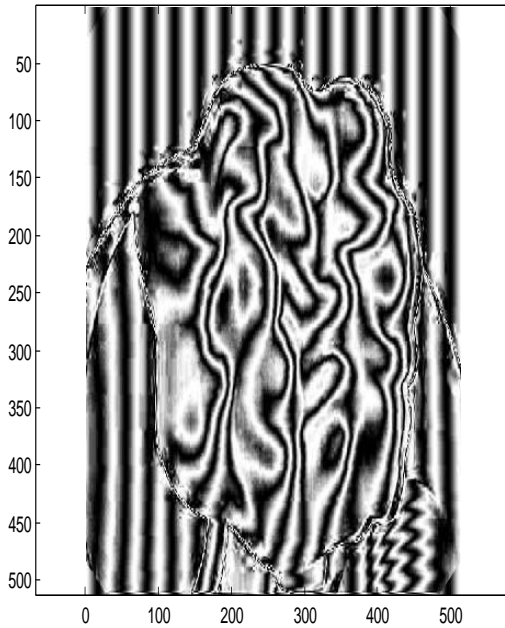


Figure (9-c): The modulated cancerous part from the kidney.

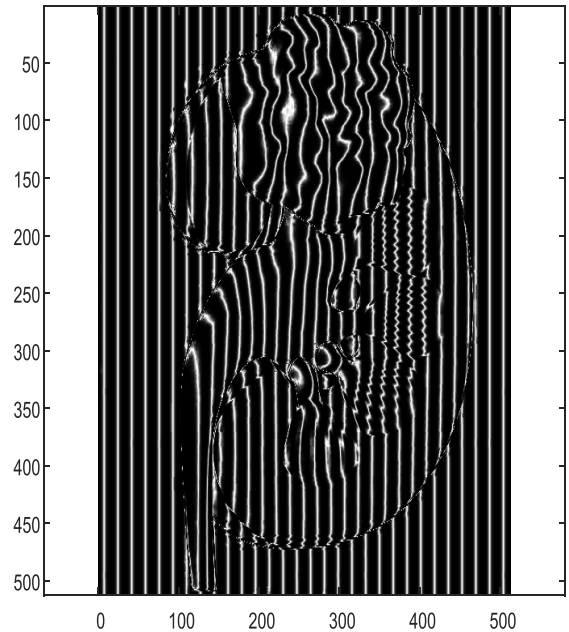


Figure (10- b): Cascaded F P I where the number of interferometers $N= 2$. The cancerous kidney shown in the figure (8- b) is modulated by 30 fringes.

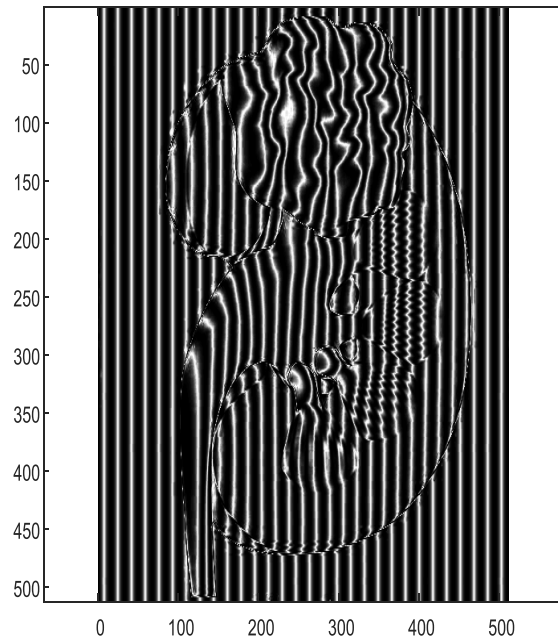


Figure (10- a): Ordinary F P I where the number of interferometers $N= 1$. The cancerous kidney shown in the figure (8- b) is modulated by 30 fringes.

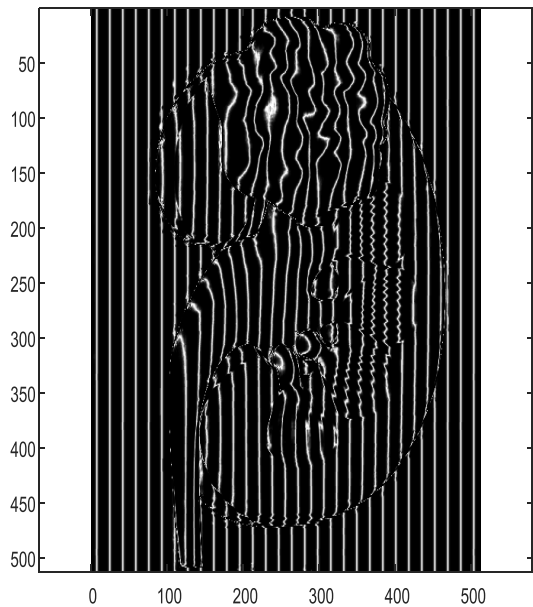


Figure (10- c): Cascaded F P I where the number of interferometers $N= 3$. The cancerous kidney shown in the figure (8- b) is modulated by 30 fringes.

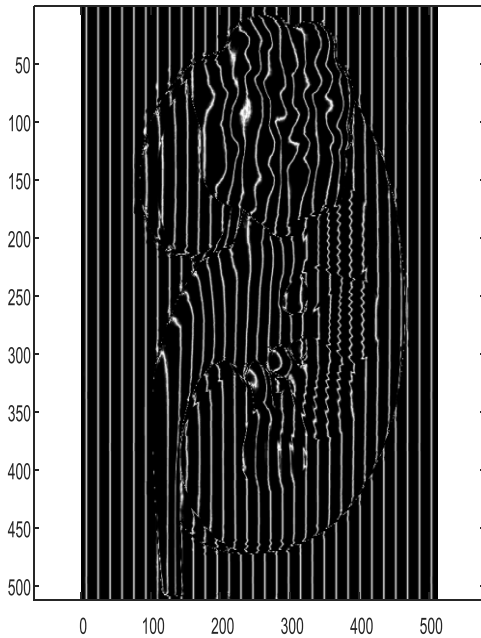


Figure (10- d): Cascaded F P I where the number of interferometers $N= 4$. The cancerous kidney shown in the figure (8- b) is modulated by 30 fringes.

4. CONCLUSION

We suggested improved CFPI using cascaded arrangement of the multiple beam interferometers. The contrast is further improved compared with the ordinary FPI. In addition, comparison of the interferometric images with the two beam interference is shown. Application on kidney images either normal or cancerous showed regular interference fringes in case of normal kidney while for the cancerous kidney contour and irregular shapes are shown in two and multiple beam respectively. The coefficient of finesse as a function of reflectivity is plotted for ordinary and cascaded F P I.

REFERENCE

- [1] Sandercock J. R.(1971): Proc. 2nd Int. Conf. Light scattering in solids, ed. M. Balkanski (Flammarion sciences, Paris, p. 9.
- [2] Ichi itoch S. and Nakamura T. (1975): Japanese J. Appl. Phys. 14, pp. 83- 86.
- [3] Kim D. Y. and Park J. W. (2004): Computer-Aided detection of kidney tumor on abdominal computed tomography scans, Acta Radiologica, 45(7), pp. 791-795.
- [4] Kolomaznik J. (2010): Fast segmentation of kidneys in CT images, presented at the WDS '10 Proceedings of Contributed Papers, Part I, pp. 70-75.
- [5] Ebrahimi S. and Mariano Vladimir Y (2015):Image Quality Improvement in Kidney Stone Detection on Computed Tomography Images, Journal of Image and Graphics, 3(1) pp. 40- 46.
- [6] Fisher W. (2004): Digital Television, A Practical Guide for Engineers, Springer-Verlag.
- [7] Papadimitriou and Bezerianos A. (1996): Multiresolution analysis and denoising of computer performance evaluation data with the wavelet transform, Journal of Systems Architecture 42, pp.55–65.
- [8] Khare A. and Tiwary U.S. (2005): International Journal of Wavelets Multiresolution and Information Processing 3, pp.477–496.
- [9] Nicolae Carmen Mariana and Moraru Luminita (2011): Annals of the University of Craiova, Mathematics and Computer Science Series Volume 38(1), pp. 27–34.
- [10] Kala Viswanath and Gunasundari R. (2014): International Conference on Advances in Computing, Communications and Informatics (ICACCI), DOI10.1109/ICACCI.2014.6968485.
- [11] Hamed A.M. (2016): Investigation of SIDA Virus (HIV) images using interferometry and speckle techniques, Int. J. Innovative Res. in Computer Science and Tech (IJRCST), 4, pp.38- 45.
- [12] Hamed A.M. (2016): Image processing of coronavirus using interferometry, Opt. and Photonics J. 6, pp.75- 86.
- [13] Hamed A.M. (2015): Topics on optical and digital image processing using holography and speckle techniques, publisher by Lulu.com, ISBN 9781329328464.
- [14] Hamed A.M. (2017): A Modified Michelson Interferometer and an Application on Microscopic Imaging, Int. J. Photonics and Optical Technology (IJPOT) 3, pp. 1- 5.